Systematic Modeling of Active Galactic Nuclei

MATTHIAS WEIDINGER[1], FELIX SPANIER[2],

[1] *Lehrstuhl für Theoretische Physik IV, Ruhr-Universität Bochum, Universitätsstr. 150, 44780 Bochum*
[2] *Centre for Space Research, Private Bag X600, Potchefstroom Campus, North-West University, Potchefstroom 2520*

mweidinger@tp4.rub.de

Abstract: The ongoing search for extragalactic gamma-ray sources reveals more and more blazars with the very high energy output dominating the synchrotron component, not to be explained as synchrotron self-Compton radiation consistently. In the present paper a self consistent hybrid model, allowing leptons and hadrons to be non-thermal emitters within the jet, is described. The model may be applied to various blazars of different subclasses from High Frequency Peaked BL Lac objects to Flat Spectrum Radio Quasars. Depending on the spectra and variability patterns the gamma rays are identified as inverse Compton up scattered photons or proton synchrotron radiation accompanied by photo-hadronic cascades during the modeling. Variability is crucial, for it reveals the highly non-linear nature of the photo-hadronic processes involved as compared to the inverse Compton case. The blazar 1 ES 1011+496 is used as an example and first complete lepto-hadronic and time-dependent results for this source are shown. Obviously only blazars identified as proton accelerators are possible production sites of extragalactic cosmic rays. These are - by far - not all, hence providing a natural explanation of the recently appearing envelope structure of the blazar sequence as different dominating particle species.

Keywords: active galactic nuclei: general, blazars, jets, acceleration of particles, Fermi-I, Fermi-II, numerical simulations, extragalactic cosmic rays

1 Introduction

Blazars have gained a lot of focus in the past decades, mainly due to the discovery of their very high energy (VHE) emission up to several TeV with Air-Cherenkov Telescopes like VERITAS, H.E.S.S. or MAGIC. Ever since more and more blazars with a redshift from almost zero up to $z = 0.536$ (3C 279 with MAGIC [6]) are revealed in the TeV regime, making a systematic investigation possible. The spectral emission of blazars, as arising from the highly boosted relativistic outflow [33], consists of two pronounced humps, with the first occurring in the optical to hard X-Rays and a second one in the γ-rays. Above that, blazar emission exhibits large amplitude variability across the whole spectrum on time scales down to minutes. With Fermi LAT allowing for a nearly all-sky survey between 20 GeV and 300 GeV the availability of multi wavelength (MWL) data is rapidly increasing. Using Fermi LAT, X-ray satellites and Air-Cherenkov telescopes, even MWL data of outbursts becomes available now, e.g. [4, 2].

Blazars are phenomenologically divided into different subclasses, based on their peak frequency and/or line-emission: Flat Spectrum Radio Quasars (FSRQs) like 3C 279 as the most luminous objects have their first peak in the near infrared to optical regime. Low and Intermediate frequency peaked BL Lac objects (LBLs and IBLs respectively) have a substantially lower luminosity, but the first hump in their SEDs is observed at higher energies. The highest photon energies, up to several TeVs, are achieved in High Frequency peaked BL Lac objects (HBLs, e.g. Mkn 501). However their luminosity seems to be the lowest among blazars. The blazar sequence introduced in 1998 [15] summarizing these observations as anti-correlation between the jet's kinetic power and the observed synchrotron peak frequency. Thus the different objects are to be explained by the variation of one jet-parameter: the jet's kinetic power. This sequence has been under debate ever since [23, 20]. Using new data it has been revisited and an envelope structure with low and high power jets seems to be occurring [20]. Hence, more than one parameter might be required to describe the different blazar flavors consistently.

HBLs are well explained by Synchrotron Self-Compton (SSC) models [14, 35] where the first peak is due to synchrotron radiation of primary electrons and the second hump arises from Compton up scattering of the synchrotron radiation by the primary electrons (IC). However LBLs and FS-RQs may not be explained within this SSC scenario. Their hard VHE radiation and wide spread of the peaks are not consistent with IC scattering of synchrotron photons [9]. The origin of the VHE emission in this subsample is still under debate: either external radiation providing additional target photons for IC scattering [13], or it is due to photo-hadronic cascades initiated by high energy protons combined with their synchrotron radiation [19, 9, 31].

In this paper we introduce a self consistent, time-dependent hybrid model co-accelerating electrons and protons due to diffusive shock acceleration (DSA) at the very same site, while taking all the relevant loss processes into account. The model can be applied to all blazar flavors, with the dominating particle species determined unbiasedly during the reproduction of the provided MWL data. Outbursts of blazars can be exploited as well to reveal hadron accelerators by identifying their highly non-linear fingerprints in the inter band light curves (e.g. typical time lags).

The lepto-hadronic modeling of the preliminary data of 1 ES 1011+496 is shown exemplarily this context, see Section 3.1. We also provide a possible flaring scenario, that would reveal the photo-hadronic nature of its VHE. A systematic modeling hence leads to a dichotomy in the kinetic power of the jet, whether it is able to accelerate protons to energies above thermal or not. In the last part we conclude with the blazar sequence and its envelope structure still be

explainable by the variation of one single parameter: the magnetic field B within the emitting region, since it is important for particle confinement, cooling and acceleration. This has impact on possible sources of extragalactic cosmic rays among AGN.

2 Model Description

We assume a spherical setup where an acceleration zone is nested within a radiation zone. As this region (blob) moves down the jet axis towards the observer with bulk Lorentz-factor Γ, upstream electrons and protons $Q_{0,i}(\gamma) = Q_{0,i}\delta(\gamma - \gamma_{0,i})$, with i being $i = e^-$ and $i = p^+$ for primary electrons and protons respectively, enter the highly turbulent acceleration zone. Here they undergo continuous DSA reaching non-thermal energies, until acceleration becomes inefficient or synchrotron losses dominate. All calculations are conveniently made in the rest-frame of the blob. Both zones are assumed to be homogeneous and to contain isotropic particle distributions as well as the same randomly orientated magnetic field B. We assume a constant acceleration efficiency of

$$t_{\mathrm{acc},i} = \left(\frac{v_s^2}{4K_{||,i}} + 2\frac{v_A^2}{9K_{||,i}}\right)^{-1} \propto m_i \qquad (1)$$

as derived from the hard sphere approximation of the underlying plasma, i.e. the spatial diffusion coefficient $K_{||}$ is energy independent [28]. With v_s and v_A as the typical shock and Alfvén speeds providing the scattering centers mandatory for efficient DSA. The acceleration timescale as free parameter is set to be proportional to the particle's typical gyrating timescale, hence to its mass in the energy independent case. The escape-time for the accelerating site is set to be constant and within the order of the accelerating timescale $t_{\mathrm{esc},i} \propto t_{\mathrm{acc},i}$ to ensure power-law particle spectra as expected from DSA [18, 34, 16]. The kinetic equations in the acceleration zone, as derived from the relativistic Vlasov equation (e.g. [29]) in the highly relativistic $p_i = \gamma_i m_i c$ case, yield:

$$\partial_t n_i = \partial_\gamma \left[(\beta_{s,i}\gamma^2 - t_{acc,i}^{-1}\gamma) \cdot n_i\right] +$$
$$\partial_\gamma \left[[(a+2)t_{acc,i}]^{-1}\gamma^2\partial_\gamma n_i\right] + Q_{0,i} - \frac{n_i}{t_{esc,i}} \quad (2)$$

with the synchrotron $\beta_{s,i} \propto Bm_i^{-3}$ and $a \propto v_s/v_A$. Note: With vanishing proton injection ($Q_{p^+} \to 0$) the model reduces to the SSC case described in [34, 35]. The shape and maximum γ_is the particles can reach arise self consistently during the modeling and are not free parameters.

Eventually all particles escaping the accelerating region enter the radiation zone, where acceleration is negligible. Here, the particles are confined long enough to ensure efficient emission. Considering p^+ this requires substantially higher B-fields of $\mathcal{O}(10\mathrm{G})$ to guarantee enough gyrations, i.e. $t_{\mathrm{gyr}} \ll t_{\mathrm{esc,rad},i}$ or simply put $r_{\mathrm{gyr}} < R_{\mathrm{rad}}$ [9, 11], within the radiation zone as compared to the SSC limit, usually assuming $\mathcal{O}(1\mathrm{G})$ [19, 34]. Highly relativistic protons with $\gamma_{p^+} > 10^5$ are subject to photo-meson production with the radiation field of the emitting region. The produced pions are unstable particles and decay into stable $e^\pm$ (and γs) via the muon channel, thereby producing neutrinos of flavors

$$\pi^+ \rightarrow \mu^+ + \nu_\mu \rightarrow e^+ + \nu_e + \nu_\mu,$$
$$\pi^- \rightarrow \mu^- + \bar{\nu}_\mu \rightarrow e^- + \bar{\nu}_e + \bar{\nu}_\mu,$$
$$\pi^0 \rightarrow \gamma + \gamma. \qquad (3)$$

The resulting stable leptons will have ultra-relativistic energies, thus their synchrotron emission, as well as the γs from the π^0 decay, result in the optically thick regime for $\gamma - \gamma \to e^\pm$ pair-production. The initiated electromagnetic cascade continues until the radiation enters the optically thin regime and can escape the blob. This emission is thus rather featureless and can contribute from X-rays to VHE, depending on the chosen set of parameters. The kinetic equation governing the evolution of $e^\pm$ in the radiation zone hence are

$$\partial_t N_{e^\pm} = \partial_\gamma \left[(\beta_{s,e}\gamma^2 + P_{IC}) \cdot N_{e^\pm}\right]$$
$$- \frac{N_{e^\pm}}{t_{rad,esc,e}} + Q_{pp} + Q_{p\gamma^\pm} + b\frac{n_{e^\pm}}{t_{esc,e}} \quad (4)$$

with $n_{e^+} = 0$ (no primary positrons), and for the protons

$$\partial_t N_{p^+} = \partial_\gamma \left[(\beta_{s,p^+}\gamma^2 + P_{p\gamma}) \cdot N_{p^+}\right]$$
$$+ b\frac{n_{p^+}}{t_{esc,p^+}} - \frac{N_{p^+}}{t_{esc,rad,p^+}} \quad (5)$$

respectively. Following the discussion of [8, 7] the loss rate of the protons due to the photo-hadronic interactions, $P_{p\gamma}$, can be neglected in most cases, leaving a relatively simple equation for the p^+, with only synchrotron losses being relevant. b is a constant geometric factor ensuring particle conservation. Analogous to the acceleration zone, we assume the escape timescale to be $t_{\mathrm{esc,rad},i} \propto m_i$. It is derived from the particle's light crossing time of the radiation zone of radius R_{rad}, multiplied by a constant empirical factor η.

To calculate the production rate of stable particles from pion production, $Q_{p\gamma^\pm}(\gamma_{e^\pm}) \propto N_{p^+}, N_{ph}$, we use [17]'s (including their Erratum) $\Phi_\pm$-parametrization of the SOPHIA Monte Carlo results [21] for these processes. Hence we assume the photo-hadronic interactions to be instantaneous compared to the synchrotron loss timescale. Even in relatively high magnetic fields this error remains small, i.e. $\tau_\mu(\gamma) \ll t_{\mathrm{syn},\mu}$ [22, 31, 11]. The pair-production rate $Q_{pp}(\gamma) \propto N_{ph}$ is calculated using the approximation eq. (12) of [10] and the IC losses $P_{IC}(\gamma_{e^\pm}) \propto N_{ph}$ exploits the full Klein-Nishina cross section. The photon distribution in the radiation zone, which is eventually beamed towards the observer to calculate the SED, reads

$$\partial_t N_{ph} = R_s + R_c + R_{\pi^0} - c(\alpha_{SSA} + \alpha_{pp})N_\gamma - \frac{N_{ph}}{t_{ph,esc}} \quad (6)$$

with the emissivities $R_c(\nu) \propto N_{e^\pm}, N_{ph}$, $R_{\pi^0}(\nu) \propto N_{p^+}, N_{ph}$, $R_s(\nu) \propto N_{e^\pm}$ for Compton scattering, neutral pion decay and synchrotron radiation respectively. The photon escape timescale is the light crossing time. R_c is calculated using the full Klein-Nishina cross section, R_{π^0} uses [17] and R_s the Melrose approximation. In optically thick regimes the photon field is absorbed either, in the low energies, due to synchrotron self absorption (α_{SSA}) for which the monochromatic approximation [35] is used or, in the VHEs, due to $e^\pm$-pair-production. The photon annihilation coefficient α_{pp} is calculated using the exact result of [12] for isotropic pair plasmas.

Within the model assumptions it is possible to explain the VHE peak in typical blazar spectra, either as inverse Compton up scattering of synchrotron photons, or as proton synchrotron radiation consistently accompanied by cascaded radiation from the photo-hadronic interactions, just dependent on the chosen parameters. Using numerical methods we can compute inter band light curves, including all nonlinearities due to the coupling of eqn. (4) - (6), making the potential information from outbursts of blazars accessible for physical interpretations.

It should be noted that merely one (two) additional parameter(s), namely the p^+/e^--ratio (and $\gamma_{0,p^+}/\gamma_{0,e^-}$) is (are) required in the model, compared to the SSC limit.

3 Results

3.1 Example: 1 ES 1011+496

The MWL observation of 1 ES 1011+496, a HBL/IBL detected at relatively high redshift of $z = 0.212$ [5], conducted March 2008 until June 2008 [27, 26] is used to emphasize the importance of hadronic models for blazar emission and as a representation for the systematic modeling conducted. The contemporaneously detected low state of 1 ES 1011+496 suggests high magnetic fields to be present in the emitting region of its jet. Hence, p^+ acceleration needs to be accounted for, making them relevant emitters in the jet. The modeling results for both i) low magnetic fields in the SSC limit and ii) a high B-field and hybrid VHE emission are shown in Fig. 1.
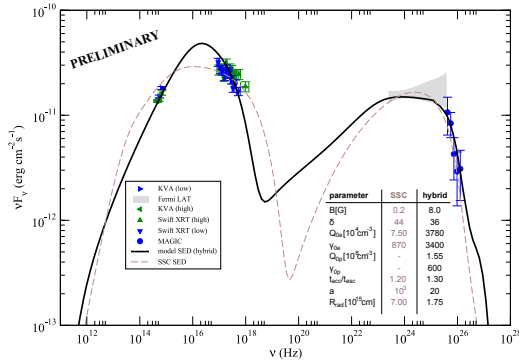

Figure 1: Leptonic (dashed brown) and hybrid (solid black) model SED with the model described in Section 2, parameters in the embedded table. Contemporaneous low state MWL data from [27] shown in blue (note that the measured TeV spectrum is used here), high state in green, the gray butterfly represents the Fermi LAT 1-yr. Cat. spectrum. The model SEDs where absorbed using the EBL model of [25].

While it is not possible to explain the highly peaked structure of the first hump with physically reasonable parameters in terms of a self consistent SSC model, it is reproduced quite well in the hybrid case, including high B-fields. The gray butterfly indicates the Fermi LAT 1-year average, used as an upper limit during the modeling, since the detection in 2008 yields a very low state of 1 ES 1011+496 [26]. To investigate the TeV emission of 1 ES 1011+496 more thoroughly it is convenient to use the intrinsic SED, unaffected by EBL, as shown in Fig. 2.

The first peak of the SED is synchrotron radiation of the primary e^- within the radiation zone. However, the situ-
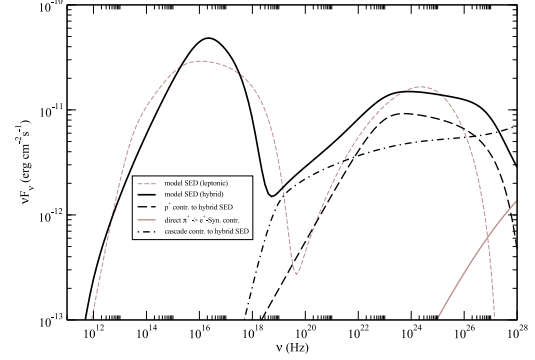

Figure 2: Intrinsic SED of 1 ES 1011+496 as modeled. Low magnetic field (SSC) case shown as dashed brown, high magnetic field (hybrid) case as solid black. First hump due to primary e^--synchrotron radiation. Individual contributions to the VHEs: p^+-synchrotron (dashed black), pair-cascaded synchrotron (dashed-dotted black) emission. Also shown: direct e^+-synchrotron component arising from π^+ decay (solid brown).

ation concerning the second hump is slightly more complex than in the SSC limit. It has two major contributions: synchrotron photons of the highly relativistic primary p^+ with Lorentz-factors up to $\gamma_p \approx 10^{10}$ and cascade radiation. The latter is synchrotron radiation of the stable products arising from photo-meson production redistributed from the optically thick regime for pair-production until observable. What might already be deduced from Fig. 2, becomes obvious in a possible flaring scenario for 1 ES 1011+496, with the resulting inter band light curves shown in Fig. 3. The flare was modeled injecting more primary particles into the considered region for a certain amount of time, motivated by density fluctuations as the blob moves along the jet. The first outburst occurring in all energy bands is due to enhanced primary e^-, leading to more synchrotron photons in the X-rays and thus providing more targets for the photo-hadronic interactions.
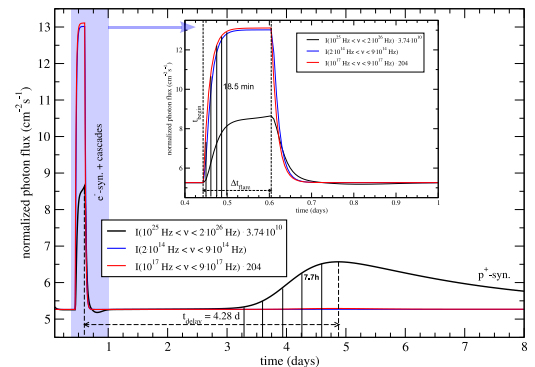

Figure 3: Inter band light curves of 1 ES 1011+496 during the imposed flaring scenario. Accompanied flare in the optical (blue), X-ray (red) and γ-ray (black) regime as accessible by e.g. KVA, Swift and Fermi respectively due to enhanced primary e^- and cascades. Orphan flare with a typical time lag due to co-accelerated p^+-synchrotron radiation. All times shown in the observer's frame.

The freshly injected p^+ on the other hand need time

$\propto t_{\text{acc},p^+}$ to accelerate to high γ_ps. As the X-Ray peak has already cooled down to its low state, the proton synchrotron contribution becomes visible as an orphan flare in the Fermi LAT energy band with a variability timescale dominated by t_{syn,p^+}. A time lag like that and typical timescales would be ideal fingerprints to discriminate leptonic against hadronic emission. Yet another advantage of the numerical treatment is the possibility to compute the overall SED at any given time during an outburst. This is especially relevant considering long flares (e.g. due to the hadronic timescales) and different photon collecting times of the various telescopes involved.

3.2 Systematic Modeling

The scenario of 1 ES 1011+496 is just one example for an outburst and the actual values for typical time lags and timescales will delicately depend on the used parameters inferred from the modeling. Even the light curves change dramatically, e.g. in the highly non-linear case with cascades extending down to X-rays being an additional target for the photo-hadronic interactions [36, 24].

We applied the method described above to ten blazars of all flavors, some of them in different flux states. The subsample of HBLs is well explained by the SSC mechanism, see [34, 36], whereas FSRQs require high magnetic fields and p^+ to be present within the jet to describe their MWL emission [31]. Intermediate and undetermined blazar flavors are sometimes explained with, but also without relativistic hadrons to be relevant emitters. The injected kinetic power in the SSC limit is in perfect agreement with studies of the Eddington-efficiency of radio loud AGN [32]. We find values up to several 10^{42} ergs^{-1}. Hadronically dominated blazars on the other hand exhibit kinetic luminosities from $L_{\text{inj}} = 10^{43}$ ergs^{-1} up to several $L_{\text{inj}} = 10^{45}$ ergs^{-1}, just below the Eddington-limit of a typical SMBH of $M_{\text{BH}} \approx 10^9 M_\odot$ in the center of an AGN. Due to p^+ confinement this naturally leads to a dichotomy in the jet's kinetic power with the magnetic field as the most important parameter. B is crucial for the synchrotron emissivity and cooling, with the peak luminosities and frequencies scaling accordingly. However, the contribution of the individual components to the overall SED, especially the pair-cascades throughout different energies, vary. Hence making it - in some cases - difficult to describe short-term variability in context of hadronic emission [36]. External radiation might play an important role in those cases, see e.g. [13, 9], needing a deeper and time-dependent investigation.

4 Conclusions

In this paper we have presented a fully time-dependent and self consistent emission model for blazars taking leptons and hadrons as potentially relevant emitters into account. The importance of the particle species is determined unbiasedly during the modeling of the individual sources. The first time-dependent results for 1 ES 1011+496, including a possible outburst do discriminate this model against external Compton models, have been shown exemplarily. From systematic modeling we can deduce that, even considering the hybrid case only, the importance of the individual components depends delicately on the chosen set of parameters. Thus, the treatment of the non-linearities due to back-reaction of the cascades on the pion production becomes inevitable in some cases. Due to that, imposed outbursts show orphan flares not only like the one of 1 ES 1011+496, but also in different energy bands.

The blazar sequence, including its recently appearing envelope structure [20], can still be described based on one single parameter, namely the magnetic field B of the emitting region when considering two potentially relevant particle species: High magnetic fields naturally lead to p^+ confinement accompanied by high kinetic luminosities. While the magnetic field scales down particles can be accelerated to higher energies, hence the synchrotron peak frequency rises as its luminosity scales down with the synchrotron emissivity. With the magnetic field being too low to confine p^+, the jet power suddenly drops explaining the second side of the blazar envelope ("decelerating jets" in [20]). If one scales the particle densities with the B-field of the jet as motivated, e.g. by self-generated magnetic fields [30], the blazar sequence and its dichotomy arises automatically, when a self consistent hybrid model is used unbiasedly. Of course further investigations, carried out in an forthcoming paper, are required to provide hard proof.

Additionally only the hybrid blazars are valid candidates for acceleration sites of UHECRs [36]. This rather general statement needs to be investigated in detail, in particular when it comes to acceleration efficiency. The maximum energy the protons can reach in typical blazars is a discussion directly related to assumed existence of the GZK cutoff in the spectrum of CRs [1, 3].

References

[1] R.U. Abbasi et al., Physical Review Letters 100(10) (2008) 101101+.
[2] A.A. Abdo et al., The Astrophysical Journal 727 (2011) 129+.
[3] J. Abraham et al., Physical Review Letters 101(6) (2008) 061101+.
[4] V.A. Acciari et al., The Astrophysical Journal 729 (2011) 2+.
[5] J. Albert et al., The Astrophysical Journal Letters 667 (2007) L21-L24.
[6] J. Albert et al., Science 320 (2008) 1752-1754.
[7] V.S. Berezinsky and S.I. Grigor'eva, A&A 199 (1988) 1-12.
[8] G.R. Blumenthal, Phys. Rev. D 1(6) (1970) 1596-1602.
[9] M. Böttcher, A. Reimer and A.P. Marscher, The Astrophysical Journal 703 (2009) 1168-1175.
[10] M. Böttcher and R. Schlickeiser, A&A 325 (1997) 866-870.
[11] M. Böttcher et al., The Astrophysical Journal 768 (2013) 54+.
[12] P.S. Coppi and R.D. Blandford, MNRAS 245 (1990) 453-507.
[13] C.D. Dermer et al., The Astrophysical Journal 692 (2009) 32-46.
[14] J.D. Finke, C.D. Dermer and M. Böttcher, The Astrophysical Journal 686 (2008) 181-194.
[15] G. Ghisellini et al., MNRAS 301 (1998) 451-468.
[16] A.M. Hillas, Annual Review of Astronomy and Astrophysics 22 (1984) 425-444.
[17] S.R. Kelner and F.A. Aharonian, Physical Review D 73(3) (2008) 034013+.
[18] J.G. Kirk et al., A&A 333 (1998) 452.
[19] K. Mannheim, A&A, 269 (1993) 67-76.
[20] E.T. Meyer et al., The Astrophysical Journal 704 (2011) 98+.
[21] A. Mücke et al., Nuclear Physics B Proceedings Supplements 80 (2000) C809+.
[22] A. Mücke et al., Astroparticle Physics 18 (2003) 593+.
[23] E. Nieppola et al., A&A 488 (2008) 867-872.
[24] M. Petropoulou and A. Mastichiadis, MNRAS 421 (2012) 2325-2341.
[25] J.R. Primack, J.S. Bullock, and R.S. Somerville, Am. Inst. Phys. Conf. Series 745 (2005) 23+.
[26] R. Reinthal et al., Journal of Physics Conference Series 355 (2012) 012017.
[27] S. Rügamer et al., Fermi Symposium Proceedings (2011)
[28] R. Schlickeiser, A&A 136 (1984) 227-236.
[29] R. Schlickeiser, Astronomy and Astrophysics Library. Berlin: Springer (2002).
[30] R. Schlickeiser and I. Lerche, A&A 476 (2007) 1-8.
[31] F. Spanier and M. Weidinger, International Journal of Modern Physics Conference Series 8 (2012) 293-298.
[32] A. Treves et al., Astron. Soc. of the Pacific Conf. Series 258 (2002) 303+.
[33] C.M. Urry, arXiv Dec. (1998).
[34] M. Weidinger et al., Astrophysics and Space Sciences Transactions 6 (2010) 1-7.
[35] M. Weidinger and F. Spanier, A&A 515 (2010) A18+.
[36] M. Weidinger and F. Spanier, Proceedings of the 32nd ICRC (2011).